Autonomous Microlasers for Profiling Extracellular Vesicles from Cancer Spheroids

Ziyihui Wang[1,2], Guocheng Fang[2]*, Zehang Gao [3,4], Yikai Liao[2], Chaoyang Gong[2], Munho Kim[2], Guo-En Chang[5], Shilun Feng[3], Tianhua Xu[1,6], Tiegen Liu[1], Yu-Cheng Chen[2]*

[1] School of Precision Instrument and Opto-Electronics Engineering, Tianjin University, Tianjin 300072, China

[2] School of Electrical and Electronics Engineering, Nanyang Technological University, 50 Nanyang Ave., Singapore 639798, Singapore

[3] State Key Laboratory of Transducer Technology, Shanghai Institute of Microsystem and Information Technology, Chinese Academy of Science, Shanghai, 200050, China

[4] Department of Clinical Laboratory, Third Affiliated Hospital of Guangzhou Medical University, Guangdong 510150, China

[5] Department of Mechanical Engineering, and Advanced Institute of Manufacturing with High-Tech Innovations, National Chung Cheng University, Chiayi 62102, Taiwan

[6] School of Engineering, University of Warwick, Coventry, CV4 7AL, United Kingdom

* Correspondence Email: *guocheng.fang@ntu.edu.sg*
yucchen@ntu.edu.sg

Abstract

Self-propelled micro/nanomotors are emergent intelligent sensors for analyzing extracellular biomarkers in circulating biological fluids. Conventional luminescent motors are often masked by highly dynamic and scattered environment, creating challenges to characterize biomarkers or subtle binding dynamics. Here we introduce a strategy to amplify subtle signals by coupling strong light-matter interactions on micromotors. A smart whispering-gallery-mode microlaser that can self-propel and analyze extracellular biomarkers is demonstrated through a liquid crystal microdroplet. Lasing spectral responses induced by cavity energy transfer were employed to reflect the abundance of protein biomarkers, generating exclusive molecular labels for cellular profiling of exosomes derived from 3D multicellular cancer spheroids. Finally, a microfluidic biosystem with different tumor-derived exosomes was employed to elaborate its sensing capability in complex environments. The proposed autonomous microlaser exhibits a promising method for both fundamental biological science and applications in drug screening, phenotyping, and organ-on-chip applications.

Keywords: self-propelled motors; microlaser; whispering gallery modes; extracellular vesicles; liquid crystal; tumor spheroids

Cell secretion is a fundamental yet critical process in cell biology in which proteins, ions, and metabolites are released into the surrounding extracellular environment. Likewise, exosomes are tiny vesicles known for carrying a multitude of bioactive cargoes (protein, DNA, and RNA) of the parent cells that travel in our body fluids.[1-3] Besides their pivotal role as biomarkers, exosomes are associated with various biological processes such as cell-cell communication, proliferation, differentiation, and therapeutics.[4, 5] However, like all other cell-secreted analytes, exosomes circulate in our tissues and blood streams with the inhomogeneous distribution. Origin differences and local concentration differences may also contribute to different levels of biomarker expressions.[6]

To address this issue, micro/nanomotors have emerged as active agents for biosensing owing to their unique ability to propel and travel in biofluids. By converting energy from the surrounding environment into autonomous movement, self-propelled motor-based biosensors have gained considerable attention.[7-12] Studies have demonstrated that the continuous movement of micromotors can enhance target binding efficiency and sensitivity, allowing direct identification and isolation of different biological targets.[13-15] The significantly improved analyte–receptor interactions can also be obtained through the increased fluid transport associated with propelled motions of micromotors. Through the integration of light-emitting fluorophores, self-propelled motors can continuously monitor and reflect the status of inhomogeneous biological micro-environment. As of today, self-propelled luminescent micro/nanomotors have been used to detect exosomes,[16] glucose,[17] proteins,[15, 18] DNA/RNA,[19, 20] endotoxin,[21], and heavy metal ions[22]. Most motor-based biosensors utilize fluorescence or chemical luminescent emissions to identify their binding events and process. Nevertheless, luminescent motors are oftentimes weak and masked by the highly dynamic and scattered biological environment from excessive fluorophores and cells, which makes it challenging to characterize multiple biomarkers or detect small but biologically critical dynamics in complex fluids or tissues. A key strategy to amplify subtle biological changes on self-propelled motors is therefore desirable.

In contrast to fluorescence emissions, stimulated emissions amplified by optical resonators have shown their great potential in scattered or deep tissue environments in terms of strong coherence and intensity, narrow linewidth, and high signal-to-noise ratio.[23-31] Thanks to its distinctive emission spectra, a number of studies have demonstrated the potential of using microscale lasers for labeling purposes in cells and tissues.[32-34] Laser-emitting particles which take advantage of whispering gallery modes (WGM) are also well known for their strong light-matter interactions on their cavity interface. Due to its high sensitivity to surrounding environment changes, WGM laser particles have been employed as molecular sensors in various applications.[28, 35, 36] What is missing is an intelligent laser particle that can self-propel and self-detect cellular secretion (*e.g.,* protein, DNA, mRNA) in a complex environment.

In this study, we introduce a self-propelled laser particle that can detect extracellular vesicles and binding dynamics in complex biological fluids at various locations (**Figure 1(a)**). The autonomous microlasers were formed and studied by utilizing liquid crystal (LC) microdroplets undergoing micellar solubilization in a surfactant solution. To obtain sensing functionality, Coumarin 6 (C6)-doped liquid crystal droplets (donor) were functionalized with antibodies to capture specific proteins on extracellular vesicles. Nile Red (NR)-labeled extracellular vesicles served as the gain medium (acceptor) to report binding events on the surface of the microcavity. Upon binding events, radiative and non-radiative energy transfer would occur on the cavity interface, causing laser emissions to shift from green emission bands to red emission bands.[37-39] By monitoring the spectrally integrated laser intensities induced by interfacial cavity energy transfer, the number of exosomes and biomarkers can be analyzed. Subsequently, self-propelled droplet microlasers were applied directly in the cellular environment, including 2D cell culture and 3D tumor spheroids. Spectral responses of the protein biomarkers were analyzed in different tumor spheroid types/subtypes (*e.g.*, A549, PANC-1, MDA-MB-231, and MCF7), generating exclusive molecular labels for cellular characterization. Finally, a microfluidic chip was used to resemble different extracellular vesicles released from different organs. Multiple self-propelling microlasers were decorated with different antibodies respectively to identify exosomes and analyze

the abundance of protein biomarkers expression simultaneously.

In this study, all the WGM microlasers were formed by using nematic liquid crystals doped with dye. To ensure all the droplets are monodisperse and uniform, LC microdroplet lasers were developed by a microfluidic chip, where surfactant solution plays a critical role in preventing coalescence. The propulsion is induced by a self-sustained gradient adsorbed on the interface between LC droplet and the surrounding liquid phase when surfactant concentrations reach above a critical micelle concentration.[40, 41] This gradient in surface energy or a spatially inhomogeneous chemical reaction leads to the internal convection of the droplet and Marangoni stresses along the interface (shown in **Figure 1(b)**), thereby creating a flow pattern.[42, 43] The polarized optical image of a self-propelled LC droplet clearly indicates a structural change in LC molecule orientations during propelling motions. The self-propelling droplet was still able to generate strong WGM lasing due to total internal reflection on its spherical surface, as shown in **Figure 1(c).** However, the slow dissolution of nematic LC molecules triggered a small blue-shift tendency in the spectrum due to stokes shift and two-photon absorption.[44, 45] Interestingly, the swimming motions and trajectories of microlaser change with the droplet diameter, including random, zigzag to straight motions (**Figure 1(d)**). This phenomenon is consistent with a phenomenological theory about self-propelled objects: linear motion becomes unstable under a large diameter or high velocity, then helical motion spontaneously appears.[46-48] Under a fixed droplet size, the velocity can also be manipulated by changing the surfactant concentrations (**Figure 1(e)**). When the surfactant concentration is too high, the process of disintegration of micelles limits the swimming motion of droplets as well. The self-propelling behavior of microlasers can address the nonuniform distribution of biotargets and promote environmental convection, which is beneficial to enhance target–substrate interactions.[49]

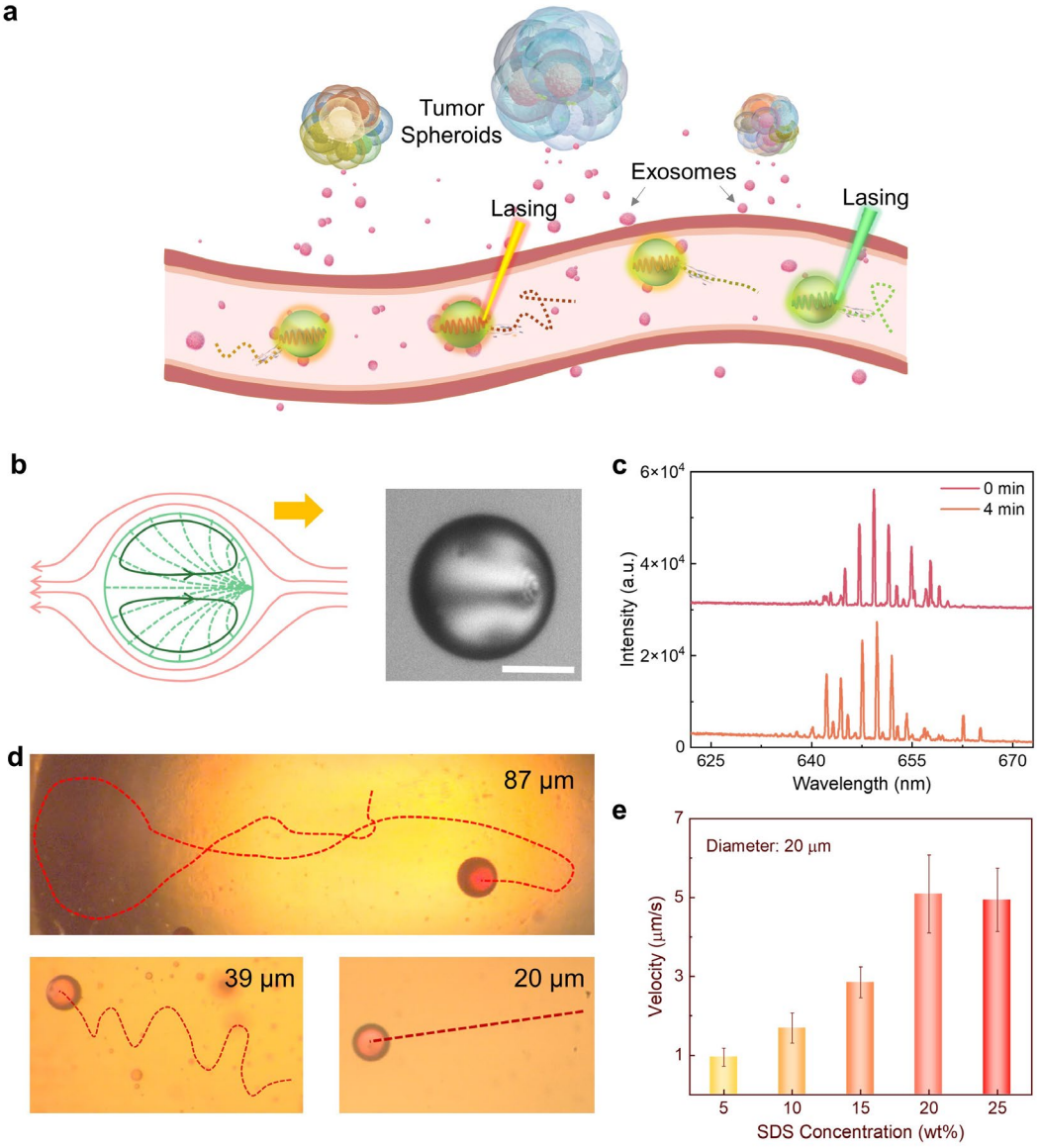

Figure 1 (a) Schematic concept of self-propelled lasers functioning as sensors in a biological fluid environment with cancer spheroid released extracellular vesicles. **(b)** Marangoni flow triggers internal convection and self-propelled motion. Left panel: Illustration of the motion direction (yellow arrow) and distorted nematic director field (green dashed lines) of the microdroplet laser. Right panel: The corresponding polarized image of the self-propelled microlaser. Scale bar: 10 μm. **(c)** Lasing emission of NR-doped lasing swimmer under 0 min and 4 min. **(d)** Typical trajectories of swimmers with various diameters. **(e)** Dependence of the velocities of 20 μm self-propelled microlaser under different SDS concentrations.

Next is how to convert self-propelled microlasers into smart probes with sensing functionality. The sensing mechanism is illustrated in **Figure 2(a)**, in which we employed interfacial energy transfer at the cavity interface to identify binding events of extracellular vesicles. Lasing microdroplets formed by C6-doped liquid crystals exhibited a strong WGM laser emission at its initial state (**Figure S1**). Before any binding events, only pure green lasing peaks (500-560nm) could be generated. No lasing signals in the red emission band exist. After red-fluorescent labeled extracellular vesicles bind to the droplet, vesicles will absorb energy from the green emission, and new lasing peaks will emerge in the red emission bands (600-650nm). Both radiative and non-radiative energy transfer plays a critical role at the microcavity interface within the distance of strong evanescent fields.[37, 39, 50] This phenomenon is due to the excellent spectral overlap between the emission band of droplet and the absorption band of exosome (**Figure S2**). Note that the exosomes carry red-fluorescent gain materials (Nile Red); hence will extend the gain profile from 550nm to 650nm when extracellular vesicles bind to the cavity surface. Benefiting from both energy transfers at the cavity interface, stronger light-matter interactions could be obtained under free-space coupling.[50]

To capture exosomes more efficiently and specifically, electrostatic interactions between poly L-lysine (PLL) and a layer of streptavidin (SA) molecules were decorated on the surface of droplet. Biotinylated-antibody functionalization was subsequently employed to capture NR-stained extracellular vesicles. To confirm lasing action from the new emerging peaks after binding, the lasing spectra and spectrally integrated output intensities from donor lasing (green) and acceptor lasing (red), were both analyzed respectively under various pump energy densities in **Figure 2(b)**. The nonlinear response of the emission intensity to the pump fluence marks the onset of lasing (**Figure 2(c)**). As seen in the inset of **Figure 2(c)**, laser emission along the circled boundary is in accordance with a typical characteristic of the WGM resonator. When the pump energy density is above the lasing threshold, significant linewidth narrowing was observed. The laser mode numbers are provided in **Figure S3** (few modes may be suppressed due to mode competition).[51-53] We also investigated the lasing thresholds of donor and acceptor after adding different concentrations of

exosomes (**Figure S4**). As the exosome (acceptor) concentration increases, more energy will be absorbed and thus, the threshold for donor droplet begins to increase, while the threshold for exosome (acceptor) decreases. To confirm that the red laser emission is not directly excited by blue pump laser, we also compared the lasing threshold of NR-stained vesicles attached to blank LC droplets (without C6 doping) in **Figure S5**. Under a fixed NR-stained vesicle concentration, a tremendously high threshold was required to achieve lasing. This result supports the existence of interfacial energy transfer from LC droplet.

We also noticed that the effect of surface-to-volume (S/V) ratio would also strongly influence detection sensitivity. [35] Higher S/V ratio, in general, should provide a higher spectral response or sensitivity under a fixed target concentration. In **Figure S6,** we compared the WGM lasing spectra generated by cavity with a diameter of 20 and 43 μm when applied with the same amount of extracellular vesicle concentration. Owing to changes in S/V ratio, it is obvious that a smaller microcavity leads to stronger lasing emission. Different S/V ratios affecting the acceptor/donor ratio will contribute to different interfacial energy transfer efficiencies and lasing intensities. Considering the influence of S/V ratio on detection sensitivity, we adopted microlasers with a cavity diameter of 20 μm (5 wt% SDS) for extracellular vesicle detections throughout the rest of this study.

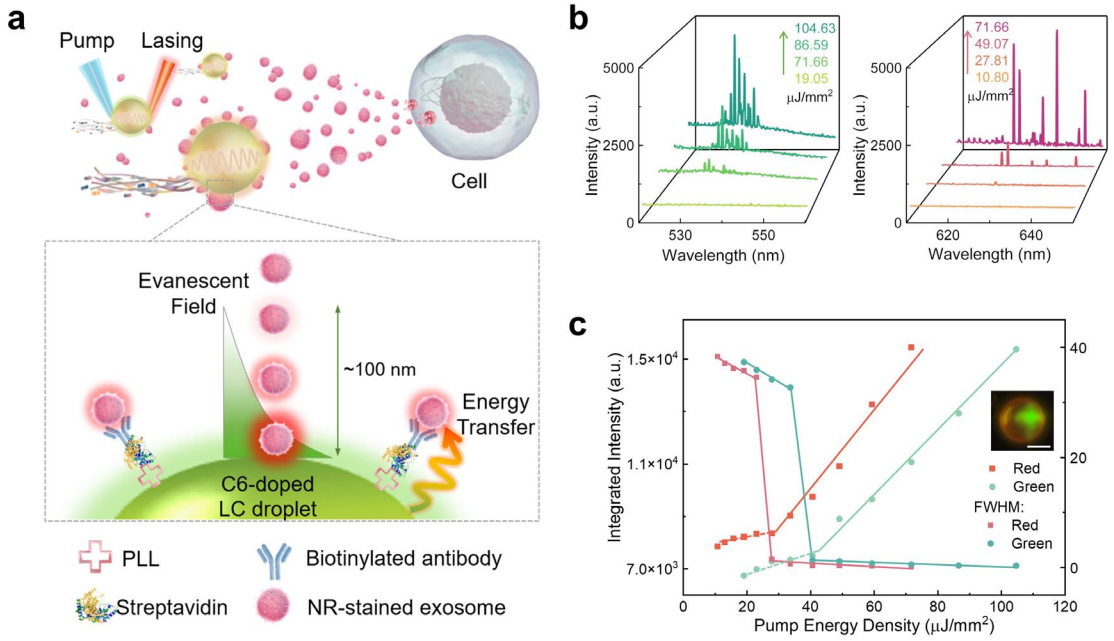

Figure 2 (a) Sensing mechanism of self-propelled microlaser for detecting cell-derived exosome. The inset shows the concept of interfacial energy transfer through cavity interface from green lasing emission to red lasing emission. **(b)** Photoluminescence spectra were recorded at the donor and acceptor lasing regions after exosome binding. Left and right panel shows lasing spectra under different pump fluences independently. **(c)** Full-width-at-half-maxima (FWHM) and derived lasing threshold plot from the green emission band (C6) and red emission band (NR). Inset: microlaser droplet after exosome binding. Scale bar: 10 μm.

Based on the above-mentioned sensing mechanism, next, we evaluated the sensing performance under different extracellular vesicle concentrations in **Figure 3**. For better quantification, purified exosomes were extracted from A549 cell culture medium by using a commercialized kit and subsequently stained with Nile Red. Detailed isolation procedures and materials are provided in Supporting Information, **Note S1**. The modal size of exosomes is approximately 79 nm, as characterized by Nanoparticle Tracing Analysis (NTA) in **Figure S7**. To demonstrate its specificity to exosomal proteins, modification of anti-CD63 on the surface of microlaser droplets was conducted. CD63 was selected because it is well-known as typical tetraspanins and exosomal markers in many cancer cells. Upon binding of exosomes, red fluorescent-stained exosomes will act as the second laser gain medium. The high binding affinity between antigen-antibody resulted

in the emergence of lasing peaks in the red emission region (600-650nm). Different concentrations of exosomes will lead to different energy transfer efficiencies at cavity interface. As presented in **Figure 3(a)**, the CCD images of self-propelled microlasers changed from green to red emission as the exosome binding increased. **Figure 3(b)** presents the lasing response of low and high densities of NR-stained exosomes. Higher concentrations of exosomes showed a higher intensity and larger redshift tendency in terms of lasing peaks than that of lower concentrations. **Figure 3(c)** shows a linear relationship between exosome concentrations and integration intensity. To elucidate the underlying mechanisms for the redshift of emergent laser emissions, the required population inversion was calculated in **Note S2** and **Figure S8**.

It is worth noting that the shift of the laser gain profile will induce inhomogeneous broadening, which may cause spectral hole burning on the resultant lasing peaks. Some lasing modes may therefore be suppressed through mode competition; however, the total integrated lasing intensity should remain the same due to energy conservation. Consequently, spectrally integrated lasing intensity in the red emission region (600-650nm) was employed to quantify the exosome binding events. To quantify the binding of exosomes, all the lasing peaks from 600-650 nm were integrated and calculated by $\int I(\lambda)\, d\lambda$, such as in **Figure S9.** $I(\lambda)$ refers to the lasing intensity at the respective emission wavelength.

To investigate the stability of microlasers, we excited the microlasers over a period of time and monitored their integrated lasing intensity. Our findings show that the integrated lasing response remains stable regardless of displacement or environmental variations (**Figure S10)**. Accordingly, we recorded all the integrated spectral responses of exosomes after 8 minutes of binding interaction with self-propelled microlasers in a cell medium. Due to energy conservation, the integrated lasing intensity remained similar regardless of mode competition in the spectrum (maximum deviation is 2.2%, which is quite acceptable). To analyse the accuracy of the proposed strategy, we compared our lasing results with the golden standard- Nanoparticle tracking analysis (NTA), under different exosome concentrations. The comparison shows the recovery rates are 93.97% and 94.35%, and the relative standard deviation was less than 9.26% (**Figure S11** and

Table S1).

To further investigate its sensitivity in complex biological fluids, various exosome concentrations were also evaluated by adding pure fetal bovine serum (FBS) to cell-derived exosomes after isolation (**Figure S12**), indicating its sensing capability of around 1.1×10^4 particles/μl. As one can see, the integrated lasing response increases quasi-linearly with the increase of exosome density, which shows that the integrated lasing response is proportional to the number of binding exosomes. By comparing the sensitivity with previous works for exosome molecular profiling in **Table S2**, our method presented a comparable sensitivity for molecular profiling in clinical samples or *in vitro* studies.

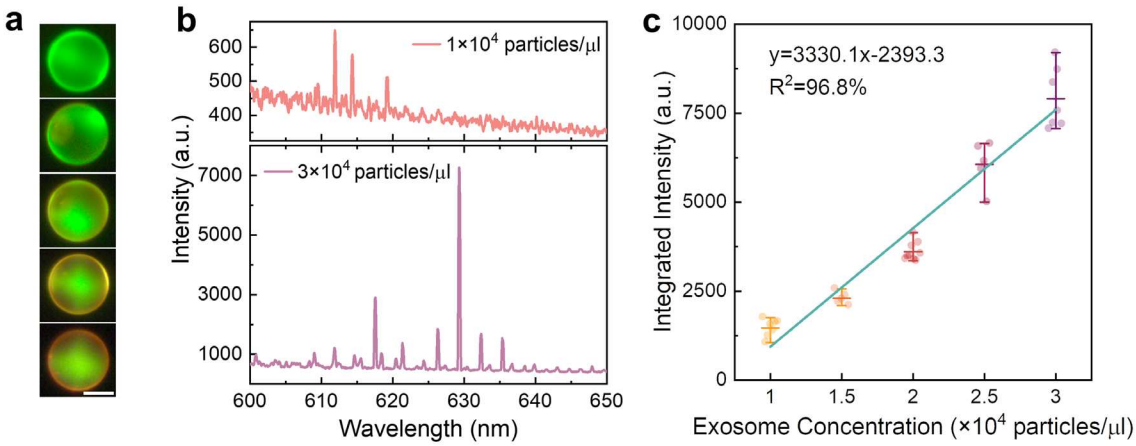

Figure 3 (a) Real-time recorded WGM lasing images of self-propelled microlaser binding with different concentrations of exosomes (from top to bottom: 1×10^4, 1.5×10^4, 2×10^4, 2.5×10^4, 3×10^4 particles/μL). Scale bar: 10 μm. **(b)** Lasing spectra of self-propelled microlaser when binding with lower and higher density of exosomes. **(c)** Spectrally integrated laser intensity (from 600 nm to 650 nm) as a function of different exosome concentrations.

Moving forward, we investigate the possibility of analyzing exosomes directly in a cellular environment (conditioned medium) without additional enrichment. Nile Red is a fluorophore that binds specifically to neutral lipids, which exhibit strong fluorescence in the presence of a

hydrophobic environment. When 2.8 nM NR is applied to conditioned medium, exosomes will be labeled by NR directly due to the lipid membrane structure of exosomes. As mentioned in **Figure 2(a)**, only exosomes binding to the cavity interface will contribute to WGM laser emissions thanks to the short distance of the evanescent field. Excessive fluorophores or unbonded exosomes can barely contribute to lasing emission. Self-propelled microlasers decorated with Anti-CD63 were therefore injected into A549 conditioned medium and recorded after 16 minutes of interactions. A stable and strong lasing emission was observed (**Figure S13**). We also evaluated the selectivity by preparing a self-propelled microlaser coated with Anti-Rabbit IgG as a control experiment. Owing to the non-specificity between antibody (human) and antigen (bovine), exosomes derived from cell medium with 10% FBS only resulted in a very weak or no lasing signal (**Figure S14**). The significant differences in the lasing spectral responses directly provide the basis for exosome detection in the cell culture medium.

Next, we utilized this approach to investigate the heterogeneity among different cell-derived exosomes. Four types of commonly used protein biomarkers (HSP70, CD9, CD63, and CD81) were selected to analyze protein expressions in A549 extracellular environment. As shown in **Figure 4(a)**, self-propelled microlasers were investigated in 2D extracellular environment as well as 3D tumor spheroid extracellular environment. By modifying the surface antibody of microlasers, the expression of various exosome biomarkers can be mapped through WGM lasing responses. **Figure 4(b)** shows the corresponding lasing spectral responses in 2D extracellular environment under an observation window of 16 minutes. From the results, it was clear that the integration intensities of WGM spectra from four protein targets all gradually increased with the incubation (reaction) time, and a linear correlation was found for all groups. Different lasing responses and slope values from the linear plot reveal the different expression levels of HSP70, CD9, CD63, and CD81 (lasing spectra provided in **Figure S15(a)**). A relatively high level of HSP70 and CD63 were detected, while a low abundance of CD9 was detected in A549-derived exosomes, which was also consistent with the previous works[54-57]. Each data point in **Figure 4(b)** was collected over five self-propelled microlasers. To investigate the repeatability of this approach, we also tested

expressions of CD9 and CD63 in A549-derived exosomes from different cell culture Petri dishes, as shown in **Figure 4(c)**. We can see that the expression level remains similar among different dishes; however, slight heterogeneity still exists owing to various microenvironment.

In addition to 2D cell culture, 3D multicellular spheroids can exactly fill the gap between 2D cell cultures and animal models, contributing to an understanding of cell mechanisms closer to human tissue physiology in drug screening (**Figure 4(a)**).[58, 59] To better mimic the complex tumor microenvironment, we analyzed the lasing spectral responses from A549 spheroid-derived exosomes by injecting self-propelled microlasers into the spheroid culture medium in **Figure 4(d)**. Four common biomarkers (HSP70, CD9, CD63, and CD81) were analyzed and compared (lasing spectra provided in **Figure S15(b)**).

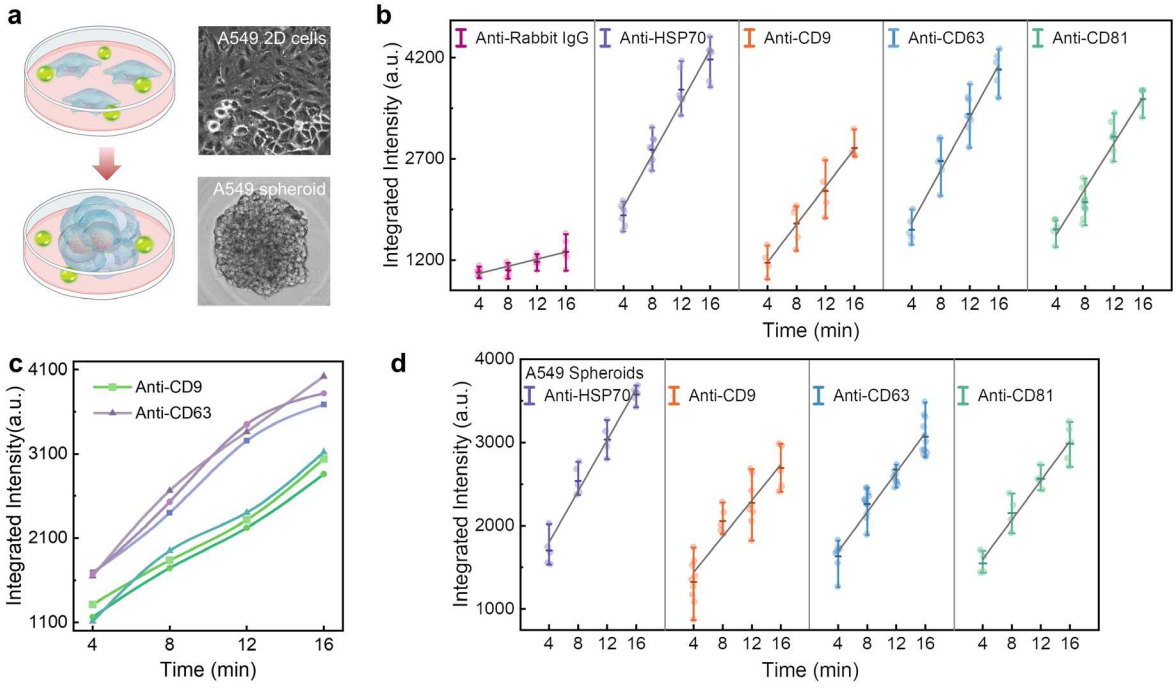

Figure 4 (a) Illustration and bright-field image of 2D cell cultures (top) and 3D tumor spheroid models (bottom). Green droplets indicate microlasers. **(b)** Statistics of lasing spectral responses measured from self-propelled microlaser with different antibodies (A549 2D cell culture-derived exosomes). **(c)** Lasing spectral response for A549-derived exosomes collected from different cell culture dish. **(d)** Statistics of lasing spectral responses measured from self-propelled microlaser

with different antibodies (A549 3D spheroid-derived exosomes).

To explore the potential of sensing exosomes in clinical samples, we prepared pooled human serum to represent health donors and human serum added with characterized exosomes from A549 to represent human patients with high-level expression of CD63 biomarker in **Figure S16.** When applying microdroplet lasers functionalized with anti-CD63 in different concentrations of A549-derived exosomes, our results demonstrated that laser spectral responses maintained a sufficient sensitivity even in human serum.

Finally, a microfluidic biosystem was built to mimic an environment with different tumor-derived exosomes, as shown in **Figure 5(a)**. The ability to identify different exosome biomarkers in a complex tumor environment is also very important. As such, three different types of multicellular 3D spheroids were cultured, respectively, including Panc-1 (pancreatic cancer cell line), MDA-MB-231 (breast cancer cell line), and MCF7 (breast cancer cell line). Extracellular mediums from three types of spheroids were then transferred to a microfluidic chip with three inlet channels (**Figure 5(b)**). Subsequently, self-propelled microlasers coated with Anti-CD9 were injected into the other end of the microfluidic chip. Microlasers will swim randomly and propel into different channels. Laser emissions are then collected and analyzed by individual droplets from each channel, resulting in the yellow color bars in **Figure 5(c)**. Similar experiments were then repeated by altering the antibody on the surface of microlaser droplets, including Anti-CD63, Anti-CD81, and Anti-HSP70. The experimental lasing spectral responses were plotted in **Figure S17** and summarized in **Figure 5(c)** in yellow, orange, pink, and purple color bars, respectively. **Figure 5(c)** provides information on exosome biomarkers detected from respective tumor spheroids in complex environments. According to the relative abundances of CD9, CD63, CD81, and HSP70, exosomes derived from 3D cancer spheroids are summarized in the heat map in **Figure 5(d)**. The heat map represents different exosome protein biomarkers (CD9, CD63, CD81, and HSP70) released in the biofluids from different 3D tumor spheroids (A549, Panc-1, MM231, and MCF-7). Heterogeneity resulting from different tumor spheroid-derived exosomes can be analyzed

through protein biomarkers on a chip.

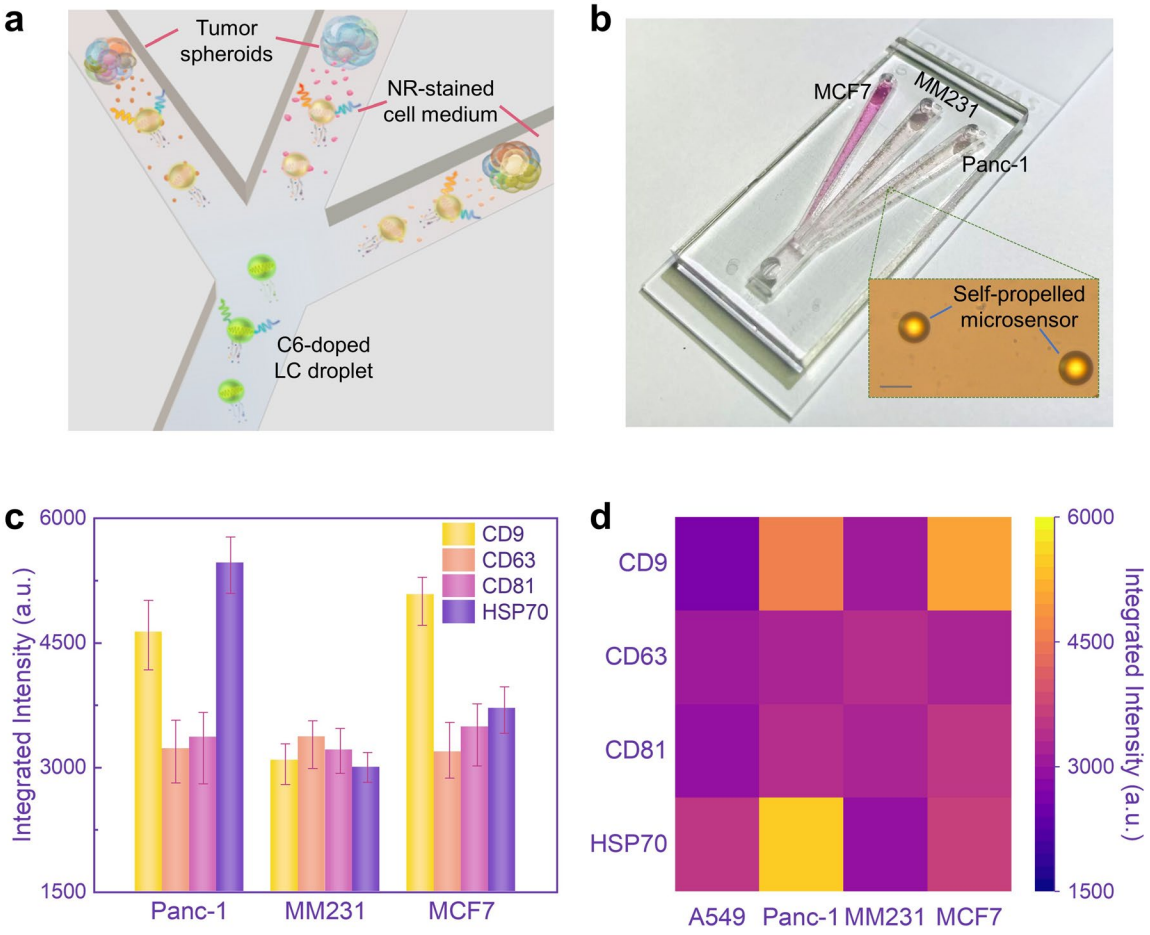

Figure 5 (a) Illustration and **(b)** image of a microfluidic chip for multiple exosome detection in an extracellular environment. Scale bar: 20 μm. **(c)** Lasing spectral responses characterizing the abundance of protein biomarker expression from Panc-1, MDA-MB-231 (MM231), and MCF7 3D tumor spheroids. **(d)** Heat map representation of different exosome protein biomarkers (CD9, CD63, CD81, and HSP70) released in the biofluids from different 3D tumor spheroids (A549, Panc-1, MM231, and MCF-7).

In this study, we developed a smart autonomous microlaser that can self-propel in a complex fluid environment and detect exosome protein biomarkers. The novel concept of integrating strong light-matter interactions on a self-propelled motor offers new opportunities to sense and amplify subtle molecular events on the fly at any location. Here we demonstrated the ability to analyze

various protein biomarkers secreted from 2D cell culture and 3D spheroid environment, even in complex environments containing different tumor-derived exosomes. Taking advantage of interfacial energy transfer on droplet cavity interface, spectrally integrated laser intensity was used as a parameter to identify the density of exosomes binding on the surface of microlasers. Our findings demonstrate that microdroplet lasers could potentially be a powerful tool to identify and amplify specific exosome binding, without the need for further enrichment or removal of excessive background dyes. The functionality of self-propelled microlasers can simply be extended to detect a wide range of cell-secreted molecules, including but not limited to mRNA, circulating DNA, and small metabolites by modifying the surface functionalization of microdroplet. The wavelength of propelled microlasers can also be flexibly designed by changing the gain material in LC droplets. Multiplexing is, therefore, a possible application due to the narrow linewidth of laser emissions. The propelling mechanism demonstrated in this work can be significantly improved and replaced by other chemical reactions in the future. Currently, the laser emission is not related to its propelling action or motions. It would be very useful if laser emission changes (wavelength shift, intensity, etc.) could be used to reflect its propelling motions related to surface reactions.

For real world applications in the future, it is more advantageous to use single-mode laser. This can be solved using WGM microlasers with higher refractive indexed materials and smaller diameters (smaller mode volume). Today, many groups have developed single-mode WGM lasers that are good enough for sensing in biological environments.[32] Another approach is establishing an imaging sensor system that can directly calibrate the wavelength shift from a camera.[60, 61] To perform in vivo sensing applications, the material of the current study can be replaced by biocompatible materials to form biolaser droplets, such as albumin or other types of liquid crystals.[62, 63] We envision the proposed study as a useful tool for fundamental biological science and applications such as drug screening and organ or tissue-on-chip applications.

Associated Content

Supporting Information

The Supporting Information is available free of charge at http://XXXXXXXXXX

Materials and Methods; Calculation of required population inversion (threshold); Table S1-Recovery experiments for exosome quantification; Table-Comparison with other methodologies for exosomes sensing; Lasing spectrum of the pure C6-doped microlaser sensor, C6-doped microdroplet after adding exosomes (without NR stained), and C6-doped microdroplet after adding the NR solution; Normalized absorption and emission spectra of dyes (C6, and NR); Mode analysis- radial (q) and angular (l) mode numbers of the microlaser; Lasing thresholds after adding low, intermediate, and high concentrations of stained exosomes measured at donor and acceptor lasing regions; Lasing threshold plots of lasing microdroplet without and with donor in droplet; Lasing spectra after applying exosomes to a microdroplet with different sizes; SEM image of A549 exosomes. Particle size distribution of exosomes characterized by NTA; Fraction of Nile Red molecules in the excited state required at lasing threshold; Illustration of the calculation of integrated intensity; Lasing responses from microlaser recorded under 3 seconds; Comparison between NTA and microlaser-based method; Spectrally integrated laser intensity (from 600 nm to 650 nm) as a function of different exosome concentrations in FBS solution; Lasing spectra of microlaser decorated with Anti-Rabbit IgG (control group) and Anti-CD63 for exosome sensing; Lasing spectral responses of antibody coated microlasers in FBS-cell medium; Lasing spectra of microlasers with different antibodies decorated for A549 cell-derived and A549 tumor spheroid-derived exosomes; Exosomes sensing in human serum with and without high-level of CD63 biomarker; Lasing spectra of microlasers with different antibodies decorated for Panc-1, MM231, and MCF7 tumor spheroid-derived exosomes; Image of microdroplet lasers fabricated by microfluidic technology; Fluorescence emission images of microcavities coated with different antibodies.

Notes

The authors declare no conflicts of interest.

Acknowledgments

This research is supported by A*STAR under its AME IRG Grant (Project No. A20E5c0085). Wang Z. would like to thank the support from China Scholarship Council (Grant No.202006250152).

Author Contributions

Z. W., G. F., and Y. -C. C. conceived and designed the experiments; Z. W., G. F., and C. G. performed the optical experiments. G. F. conducted the cellular preparation and experiments. S. F., G-E. C., and Z.

G. designed and fabricated the microfluidic devices. Z. W. and Y. -C. C analyzed the data. Y.K. and M.K. provided the support for SEM images and equipment. T. X. and T. L. provided useful advice and supporting resources. Z. W. and Y. -C. C wrote the paper. Y. -C. C. supervised the whole research.

References

(1) Kalluri, R.; LeBleu, V. S. The biology, function, and biomedical applications of exosomes. *Science* **2020**, *367* (6478).

(2) Zhang, W.; Jiang, L.; Diefenbach, R. J.; Campbell, D. H.; Walsh, B. J.; Packer, N. H.; Wang, Y. Enabling Sensitive Phenotypic Profiling of Cancer-Derived Small Extracellular Vesicles Using Surface-Enhanced Raman Spectroscopy Nanotags. *ACS Sens* **2020**, *5* (3), 764-771.

(3) Wu, D.; Yan, J.; Shen, X.; Sun, Y.; Thulin, M.; Cai, Y.; Wik, L.; Shen, Q.; Oelrich, J.; Qian, X.; et al. Profiling surface proteins on individual exosomes using a proximity barcoding assay. *Nat Commun* **2019**, *10* (1), 3854.

(4) Amrollahi, P.; Zheng, W.; Monk, C.; Li, C. Z.; Hu, T. Y. Nanoplasmonic Sensor Approaches for Sensitive Detection of Disease-Associated Exosomes. *ACS Appl Bio Mater* **2021**, *4* (9), 6589-6603.

(5) Wang, Y.; Zhang, Q.; Yuan, W.; Wang, Y.; Loghry, H. J.; Zhao, Z.; Kimber, M. J.; Dong, L.; Lu, M. Hyperspectral imaging-based exosome microarray for rapid molecular profiling of extracellular vesicles. *Lab Chip* **2021**, *21* (1), 196-204.

(6) Wang, Y.; Zhang, K.; Huang, X.; Qiao, L.; Liu, B. Mass Spectrometry Imaging of Mass Tag Immunoassay Enables the Quantitative Profiling of Biomarkers from Dozens of Exosomes. *Anal Chem* **2021**, *93* (2), 709-714.

(7) Wang, Z.; Shang, L.; Gao, Z.; Chan, K. K.; Gong, C.; Wang, C.; Xu, T.; Liu, T.; Feng, S.; Chen, Y.-C. Motor-like microlasers functioning in biological fluids. *Lab Chip* **2022**, *22* (19), 3668-3675.

(8) Yuan, K.; Cuntín-Abal, C.; Jurado-Sánchez, B.; Escarpa, A. Smartphone-Based Janus Micromotors Strategy for Motion-Based Detection of Glutathione. *Anal Chem* **2021**, *93* (49), 16385-16392.

(9) Yuan, K.; de la Asunción-Nadal, V.; Cuntín-Abal, C.; Jurado-Sánchez, B.; Escarpa, A. On-board smartphone micromotor-based fluorescence assays. *Lab Chip* **2022**, *22* (5), 928-935.

(10) Maria-Hormigos, R.; Jurado-Sánchez, B.; Escarpa, A. Biocompatible micromotors for biosensing. *Anal. Bioanal. Chem* **2022**, *414* (24), 7035-7049.

(11) Park, S.; Yossifon, G. Micromotor-Based Biosensing Using Directed Transport of Functionalized Beads. *ACS Sens* **2020**, *5* (4), 936-942.

(12) Pacheco, M.; Lopez, M. A.; Jurado-Sanchez, B.; Escarpa, A. Self-propelled micromachines for analytical sensing: a critical review. *Anal Bioanal Chem* **2019**, *411* (25), 6561-6573.

(13) Kagan, D.; Campuzano, S.; Balasubramanian, S.; Kuralay, F.; Flechsig, G.-U.; Wang, J. Functionalized Micromachines for Selective and Rapid Isolation of Nucleic Acid Targets from Complex Samples. *Nano Lett* **2011**, *11* (5), 2083-2087.

(14) Li, J.; Esteban-Fernández de Ávila, B.; Gao, W.; Zhang, L.; Wang, J. Micro/nanorobots for biomedicine: Delivery, surgery, sensing, and detoxification. *Sci. Robot.***2017**, *2* (4), eaam6431.

(15) Morales-Narváez, E.; Guix, M.; Medina-Sánchez, M.; Mayorga-Martinez, C. C.; Merkoçi, A. Micromotor Enhanced Microarray Technology for Protein Detection. *Small* **2014**, *10* (13), 2542-2548.

(16) Zhu, N.; Li, G.; Zhou, J.; Zhang, Y.; Kang, K.; Ying, B.; Yi, Q.; Wu, Y. A light-up fluorescence resonance energy transfer magnetic aptamer-sensor for ultra-sensitive lung cancer exosome detection. *J Mater Chem B* **2021**, *9* (10),

2483-2493.
(17) Sentic, M.; Arbault, S.; Goudeau, B.; Manojlovic, D.; Kuhn, A.; Bouffier, L.; Sojic, N. Electrochemiluminescent swimmers for dynamic enzymatic sensing. *ChemComm* **2014**, *50* (71), 10202-10205.
(18) Orozco, J.; Cortés, A.; Cheng, G.; Sattayasamitsathit, S.; Gao, W.; Feng, X.; Shen, Y.; Wang, J. Molecularly Imprinted Polymer-Based Catalytic Micromotors for Selective Protein Transport. *J. Am. Chem. Soc.* **2013**, *135* (14), 5336-5339.
(19) Xu, T.; Luo, Y.; Liu, C.; Zhang, X.; Wang, S. Integrated Ultrasonic Aggregation-Induced Enrichment with Raman Enhancement for Ultrasensitive and Rapid Biosensing. *Anal Chem* **2020**, *92* (11), 7816-7821.
(20) Esteban-Fernández de Ávila, B.; Martín, A.; Soto, F.; Lopez-Ramirez, M. A.; Campuzano, S.; Vásquez-Machado, G. M.; Gao, W.; Zhang, L.; Wang, J. Single Cell Real-Time miRNAs Sensing Based on Nanomotors. *ACS Nano* **2015**, *9* (7), 6756-6764.
(21) Jurado-Sánchez, B.; Pacheco, M.; Rojo, J.; Escarpa, A. Magnetocatalytic Graphene Quantum Dots Janus Micromotors for Bacterial Endotoxin Detection. *Angew. Chem. Int. Ed.* **2017**, *56* (24), 6957-6961.
(22) Jurado-Sánchez, B.; Escarpa, A.; Wang, J. Lighting up micromotors with quantum dots for smart chemical sensing. *ChemComm* **2015**, *51* (74), 14088-14091.
(23) Chen, Y.-C.; Fan, X. Biological Lasers for Biomedical Applications. *Adv. Opt. Mater.* **2019**, *7* (17), 1900377.
(24) Chen, Y.-C.; Chen, Q.; Fan, X. Lasing in blood. *Optica* **2016**, *3* (8), 809-815.
(25) Humar, M.; Dobravec, A.; Zhao, X.; Yun, S. H. Biomaterial microlasers implantable in the cornea, skin, and blood. *Optica* **2017**, *4* (9), 1080-1085.
(26) Fan, X.; Yun, S.-H. The potential of optofluidic biolasers. *Nat Methods* **2014**, *11* (2), 141-147.
(27) Zhang, Y.; Zhang, C.; Fan, Y.; Liu, Z.; Hu, F.; Zhao, Y. S. Smart Protein-Based Biolasers: An Alternative Way to Protein Conformation Detection. *ACS Appl. Mater. Interfaces* **2021**, *13* (16), 19187-19192.
(28) Toropov, N.; Cabello, G.; Serrano, M. P.; Gutha, R. R.; Rafti, M.; Vollmer, F. Review of biosensing with whispering-gallery mode lasers. *Light Sci Appl* **2021**, *10* (1), 42.
(29) Toropov, N.; Vollmer, F. Whispering-gallery microlasers for cell tagging and barcoding: the prospects for in vivo biosensing. *Light Sci Appl* **2021**, *10* (1), 77.
(30) Yuan, Z.; Cheng, X.; Zhou, Y.; Tan, X.; Gong, X.; Rivy, H.; Gong, C.; Fan, X.; Wang, W.-J.; Chen, Y.-C. Distinguishing Small Molecules in Microcavity with Molecular Laser Polarization. *ACS Photonics* **2020**, *7* (8), 1908-1914.
(31) Zhang, Y.; Yuan, Z.; Qiao, Z.; Barshilia, D.; Wang, W.; Chang, G.-E.; Chen, Y.-C. Tunable Microlasers Modulated by Intracavity Spherical Confinement with Chiral Liquid Crystal. *Adv. Opt. Mater.* **2020**, *8* (10), 1902184.
(32) Martino, N.; Kwok, S. J. J.; Liapis, A. C.; Forward, S.; Jang, H.; Kim, H.-M.; Wu, S. J.; Wu, J.; Dannenberg, P. H.; Jang, S.-J.; et al. Wavelength-encoded laser particles for massively multiplexed cell tagging. *Nat. Photonics* **2019**, *13* (10), 720-727.
(33) Fikouras, A. H.; Schubert, M.; Karl, M.; Kumar, J. D.; Powis, S. J.; Di Falco, A.; Gather, M. C. Non-obstructive intracellular nanolasers. *Nat. Commun.* **2018**, *9* (1), 4817.
(34) Haehnle, B.; Lamla, M.; Sparrer, K. M. J.; Gather, M. C.; Kuehne, A. J. C. Narrow Stimulated Resonance Raman Scattering and WGM Lasing in Small Conjugated Polymer Particles for Live Cell Tagging and Tracking. *Adv. Opt. Mater.* **2021**, *9* (4), 2001553.
(35) Wang, Z.; Zhang, Y.; Gong, X.; Yuan, Z.; Feng, S.; Xu, T.; Liu, T.; Chen, Y.-C. Bio-electrostatic sensitive droplet lasers for molecular detection. *Nanoscale Adv.* **2020**, *2* (7), 2713-2719.

(36) Schubert, M.; Woolfson, L.; Barnard, I. R. M.; Dorward, A. M.; Casement, B.; Morton, A.; Robertson, G. B.; Appleton, P. L.; Miles, G. B.; Tucker, C. S.; et al. Monitoring contractility in cardiac tissue with cellular resolution using biointegrated microlasers. *Nat. Photonics* **2020**, *14* (7), 452-458.

(37) Yuan, Z.; Wang, Z.; Guan, P.; Wu, X.; Chen, Y.-C. Lasing-Encoded Microsensor Driven by Interfacial Cavity Resonance Energy Transfer. *Adv. Opt. Mater.* **2020**, *8* (7), 1901596.

(38) Zhou, Y.; Yuan, Z.; Gong, X.; Birowosuto, M.; Dang, C.; Chen, Y.-C. Dynamic photonic barcodes for molecular detection based on cavity-enhanced energy transfer. *Adv. Photonics* **2020**, *2* (6), 066002.

(39) Jana, S.; Xu, X.; Klymchenko, A.; Reisch, A.; Pons, T. Microcavity-Enhanced Fluorescence Energy Transfer from Quantum Dot Excited Whispering Gallery Modes to Acceptor Dye Nanoparticles. *ACS Nano* **2021**, *15* (1), 1445-1453.

(40) Peddireddy, K.; Kumar, P.; Thutupalli, S.; Herminghaus, S.; Bahr, C. Solubilization of Thermotropic Liquid Crystal Compounds in Aqueous Surfactant Solutions. *Langmuir* **2012**, *28* (34), 12426-12431.

(41) Brake, J. M.; Mezera, A. D.; Abbott, N. L. Effect of Surfactant Structure on the Orientation of Liquid Crystals at Aqueous−Liquid Crystal Interfaces. *Langmuir* **2003**, *19* (16), 6436-6442.

(42) Kruger, C.; Klos, G.; Bahr, C.; Maass, C. C. Curling Liquid Crystal Microswimmers: A Cascade of Spontaneous Symmetry Breaking. *Phys Rev Lett* **2016**, *117* (4), 048003.

(43) Herminghaus, S.; Maass, C. C.; Kruger, C.; Thutupalli, S.; Goehring, L.; Bahr, C. Interfacial mechanisms in active emulsions. *Soft Matter* **2014**, *10* (36), 7008-7022.

(44) Chen, X.; Xie, K.; Hu, T.; Zhang, X.; Yang, Y.; Ma, J.; Zhang, J.; Cheng, X.; Hu, Z. Whispering gallery mode microlaser based on a single polymer fiber fabricated by electrospinning. *J. Phys. D: Appl. Phys.* **2019**, *52* (47), 475104.

(45) Peter, J.; Radhakrishnan, P.; Nampoori, V.; Kailasnath, M. Multimode laser emission from free-standing cylindrical microcavities. *J. Lumin.* **2014**, *149*, 204-207.

(46) Takabatake, F.; Magome, N.; Ichikawa, M.; Yoshikawa, K. Spontaneous mode-selection in the self-propelled motion of a solid/liquid composite driven by interfacial instability. *J. Chem. Phys.* **2011**, *134* (11), 114704.

(47) Hiraiwa, T.; Shitara, K.; Ohta, T. Dynamics of a deformable self-propelled particle in three dimensions. *Soft Matter* **2011**, *7* (7), 3083-3086.

(48) Suga, M.; Suda, S.; Ichikawa, M.; Kimura, Y. Self-propelled motion switching in nematic liquid crystal droplets in aqueous surfactant solutions. *Phys Rev E* **2018**, *97* (6-1), 062703.

(49) Moreno-Guzman, M.; Jodra, A.; López, M.-Á.; Escarpa, A. Self-Propelled Enzyme-Based Motors for Smart Mobile Electrochemical and Optical Biosensing. *Anal Chem* **2015**, *87* (24), 12380-12386.

(50) Wang, Y.; Lang, M. C.; Lu, J.; Suo, M.; Du, M.; Hou, Y.; Wang, X.-H.; Wang, P. Demonstration of intracellular real-time molecular quantification via FRET-enhanced optical microcavity. *Nat. Commun.* **2022**, *13* (1), 6685.

(51) Lam, C. C.; Leung, P. T.; Young, K. Explicit asymptotic formulas for the positions, widths, and strengths of resonances in Mie scattering. *J. Opt. Soc. Am. B* **1992**, *9* (9), 1585-1592.

(52) Tang, S. K. Y.; Derda, R.; Quan, Q.; Lončar, M.; Whitesides, G. M. Continuously tunable microdroplet-laser in a microfluidic channel. *Opt. Express* **2011**, *19* (3), 2204-2215.

(53) Wang, Z.; Liu, Y.; Gong, C.; Yuan, Z.; Shen, L.; Chang, P.; Liu, K.; Xu, T.; Jiang, J.; Chen, Y.-C.; et al. Liquid crystal-amplified optofluidic biosensor for ultra-highly sensitive and stable protein assay. *PhotoniX* **2021**, *2* (1), 18.

(54) Fan, Y.; Duan, X.; Zhao, M.; Wei, X.; Wu, J.; Chen, W.; Liu, P.; Cheng, W.; Cheng, Q.; Ding, S. High-sensitive and multiplex biosensing assay of NSCLC-derived exosomes via different recognition sites based on SPRi array. *Biosens. Bioelectron.* **2020**, *154*, 112066.

(55) Wu, D.; Yan, J.; Shen, X.; Sun, Y.; Thulin, M.; Cai, Y.; Wik, L.; Shen, Q.; Oelrich, J.; Qian, X.; et al. Profiling surface proteins on individual exosomes using a proximity barcoding assay. *Nat. Communications* **2019**, *10* (1), 3854.
(56) Li, J.; Li, Y.; Chen, S.; Duan, W.; Kong, X.; Wang, Y.; Zhou, L.; Li, P.; Zhang, C.; Du, L.; et al. Highly Sensitive Exosome Detection for Early Diagnosis of Pancreatic Cancer Using Immunoassay Based on Hierarchical Surface-Enhanced Raman Scattering Substrate. *Small Methods* **2022**, *6* (6), 2200154.
(57) Liang, M.; Chen, X.; Wang, L.; Qin, L.; Wang, H.; Sun, Z.; Zhao, W.; Geng, B. Cancer-derived exosomal TRIM59 regulates macrophage NLRP3 inflammasome activation to promote lung cancer progression. *J. Exp. Clin. Cancer Res.* **2020**, *39* (1), 176.
(58) Nunes, A. S.; Barros, A. S.; Costa, E. C.; Moreira, A. F.; Correia, I. J. 3D tumor spheroids as in vitro models to mimic in vivo human solid tumors resistance to therapeutic drugs. *Biotechnol. Bioeng.* **2019**, *116* (1), 206-226.
(59) Fang, G.; Lu, H.; Law, A.; Gallego-Ortega, D.; Jin, D.; Lin, G. Gradient-sized control of tumor spheroids on a single chip. *Lab Chip* **2019**, *19* (24), 4093-4103.
(60) Chan, K. K.; Shang, L.-W.; Qiao, Z.; Liao, Y.; Kim, M.; Chen, Y.-C. Monitoring Amyloidogenesis with a 3D Deep-Learning-Guided Biolaser Imaging Array. *Nano Lett* **2022**, *22* (22), 8949-8956.
(61) Yesilkoy, F.; Arvelo, E. R.; Jahani, Y.; Liu, M.; Tittl, A.; Cevher, V.; Kivshar, Y.; Altug, H. Ultrasensitive hyperspectral imaging and biodetection enabled by dielectric metasurfaces. *Nat. Photonics* **2019**, *13* (6), 390-396.
(62) Nguyen, T. V.; Pham, N. V.; Mai, H. H.; Duong, D. C.; Le, H. H.; Sapienza, R.; Ta, V.-D. Protein-based microsphere biolasers fabricated by dehydration. *Soft Matter* **2019**, *15* (47), 9721-9726.
(63) Franklin, D.; Ueltschi, T.; Carlini, A.; Yao, S.; Reeder, J.; Richards, B.; Van Duyne, R. P.; Rogers, J. A. Bioresorbable Microdroplet Lasers as Injectable Systems for Transient Thermal Sensing and Modulation. *ACS Nano* **2021**, *15* (2), 2327-2339.

TOC Graphic

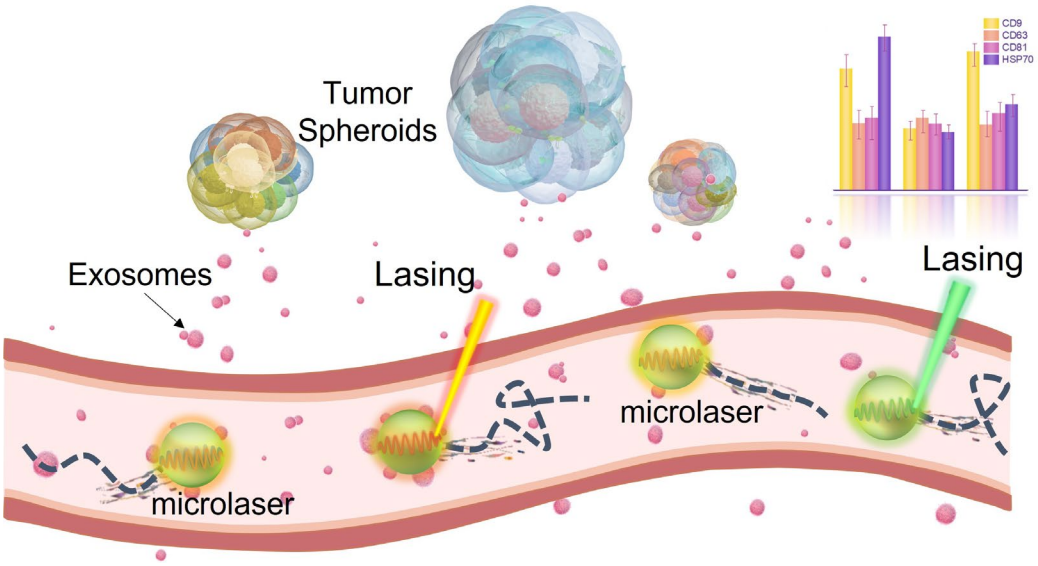
Tumor
Spheroids
CD9
CD63
CD81
HSP70
Exosomes
Lasing
Lasing
microlaser
microlaser